Aerodynamic Characteristics of a Stationary Savonius Rotor

A.K.M. Sadrul Islam, Md. Quamrul Islam, A.C. Mandal and M.M. Razzaque
Dept. of Mechanical Engineering
Bangladesh University of Engineering & Technology
Dhaka, Bangladesh

Abstract

Static torque and drag coefficients of a Savonius rotor have been investigated by measuring the pressure distribution on the blade surfaces for various rotor angles. Experiments have been performed at a Reynolds number of $2x10^5$ with a rotor having two semi-circular blades with an overlap ratio of 0.2. Results indicate that the static torque and drag coefficients vary considerably with the rotor angle. The results facilitate predicting the performance of this type of rotor under dynamic conditions.

INTRODUCTION

The Savonius rotor has been a subject of interest since the 1930's and has been studied extensively. It is a vertical axis wind turbine and has a lower efficiency compared to other vertical wind power extracting machines such as the Darrieus rotor. Nevertheless, it is used as an alternative to wind power extraction because of its simple design and good starting torque at low wind speeds [1,7,8,10]. Rigorous studies on the performance characteristics of the Savonius rotor are found in the literature and these enable the identification of an optimum geometrical configuration for practical design [2,3,6,9,11]. However, only a few studies [4,5] are reported in the literature which give information regarding the total aerodynamic load on the structure and the mechanism of rotation of the rotor. Table 1 describes the experimental parameters of these works. This paper reports an experimental study on the aerodynamic load on a stationary Savonius rotor and the mechanism of torque production by measuring the forces acting on the blades.

EXPERIMENTAL SET-UP AND PROCEDURE

The schematic diagram of the experimental set-up is shown in Fig. 1.

The tests were carried out in a uniform flow jet produced by an open circuit wind tunnel. The exit of the wind tunnel consists of a square section nozzle with a side length of 500 mm. The rotor was placed at the jet axis and 750 mm downstream of the nozzle exit. The measured mean velocity distribution at this section without the rotor was uniform to within ±0.5% of the mean velocity in the central region of 320 mm x 320 mm section. The exit velocity of the nozzle could be adjusted between 0 to 15 m/s but the present study was carried out at a constant wind speed of U_o = 13.3 m/s, i.e. at Reynolds number, Re = 2 x 10^5.

Table 1. Experimental parameters used in selected studies.

References	Re	S
Sawada et al. [4]	2.7×10^4	0.21
Fujisawa [5]	5.4×10^4	0.15
Fujisawa [5]	4.5×10^4	0.30

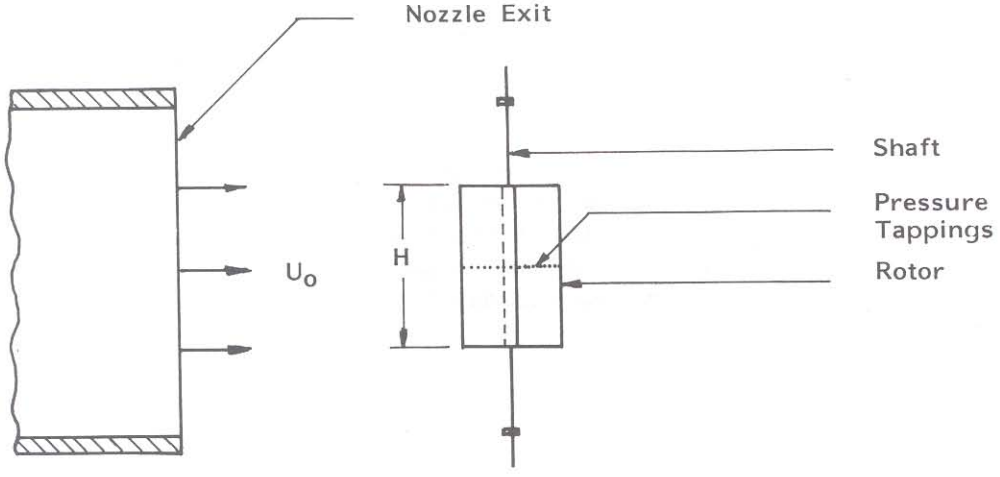

Fig. 1. Experimental set-up.

The Savonius rotor was made up of two half cylinders (blade) of diameter, d = 125 mm and height, H = 300 mm. The cylinders were made of PVC material. The overlap distance S was selected to be one-fifth of the cylinder diameter (i.e. $S = a/d = 0.2$) and the central shaft had been removed. The overlap distance selected was the optimum value with respect to the wind power extraction [3].

The pressure measurements were made at 17 pressure tappings on each blade. The tappings were located at the mid-plane of one side of each blade, so that pressure distribution at every 10° on the blade surface could be measured. The pressure tappings were connected to a pressure transducer (make : Furness Controls Ltd., UK, model : FC012) through 2 mm PVC tubes. The pressure transducer had been calibrated and had an accuracy of ±0.1 mm of water column. The pressures were measured at every 15° interval of rotor angle (Fig. 2), so that a detailed picture of the aerodynamic loading and torque characteristics could be obtained.

At a particular rotor angle, α the rotor blades experience forces (per unit span length) due to the pressure difference between the concave surface and convex surface and these forces can be resolved into two components F_n and F_t. Since the blade surfaces are circular, F_n and F_t pass through the centre of the semicircle. The positive direction of F_n and F_t are shown in Fig. 2. The drag coefficients in normal and tangential directions can be written as follows :

$$C_n = \frac{F_n}{\frac{1}{2}\rho U_o^2 d} \quad , \quad C_t = \frac{F_t}{\frac{1}{2}\rho U_o^2 d} \tag{1}$$

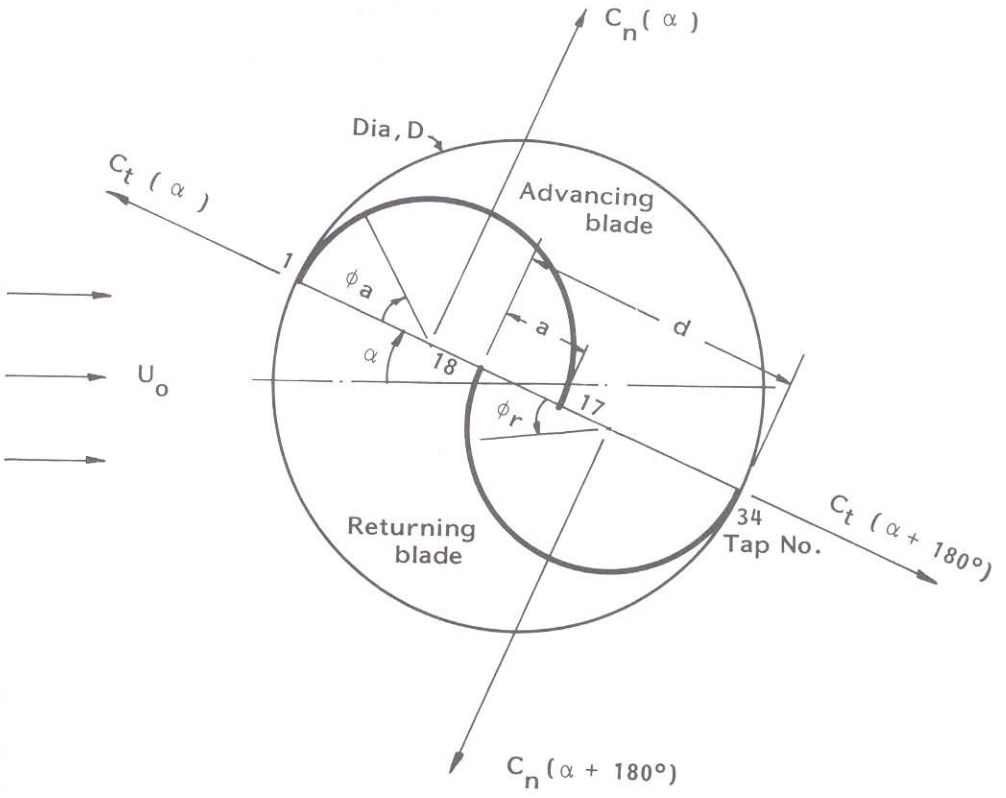

Fig. 2. Forces acting on the blades.

To obtain the drag coefficients in the normal and tangential direction of the chord, the values of F_n and F_t must be known beforehand. The values of the forces F_n and F_t are obtained by integrating the pressure for a blade as follows :

$$F_n = \int_0^{\pi} \Delta p \frac{d}{2} \cos\phi \, d\phi = \sum_{i=1}^{17} \Delta p_i \frac{d}{2} \cos\phi_i \, \Delta\phi_i \qquad (2)$$

and similarly,

$$F_t = \sum_{i=1}^{17} \Delta p_i \frac{d}{2} \sin\phi_i \, \Delta\phi_i$$

where Δp_i is the difference in pressure on the concave and convex surfaces at a particular pressure tapping, i.

Force F_n is responsible for producing a torque on the shaft of the rotor and this torque can be expressed for a blade as :

$$T = F_n * \frac{d}{2} * (1 - S) \qquad (3)$$

Equation (3) can be reduced to get the torque coefficient for a single blade at a particular rotor angle as:

$$C_q(\alpha) = C_n(\alpha)\frac{1 - S}{2 - S} \tag{4}$$

The total static torque coefficient produced on the rotor shaft can be expressed as follows:

$$C_Q(\alpha) = \left[C_n(\alpha) + C_n(\alpha + 180^\circ)\right]\frac{1 - S}{(2 - S)^2} \tag{5}$$

where $C_n(\alpha)$ and $C_n(\alpha + 180^\circ)$ refer to the drag coefficients of the advancing blade and returning blade respectively at rotor angle α.

RESULTS AND DISCUSSION

Static Aerodynamic Characteristics

The pressure distribution over the surfaces of the blades were measured at every 15° interval of rotor angle between $0^\circ \le \alpha \le 180^\circ$. Only the typical results are presented in Figs. 3(a) to 3(d) for $\alpha = 0^\circ$, 45°, 90° and 135° respectively. At $\alpha = 0^\circ$ (Fig. 3(a)) as the flow accelerates over the leading edge of the convex surface of the advancing blade, the pressure decreases up to $\phi_a = 60^\circ$ and at around $\phi_a = 70^\circ$ the flow separates as caused by an adverse pressure gradient. Then the pressure remains at a constant negative value for $80^\circ < \phi_a < 180^\circ$. On the concave surface of the advancing blade the pressure is almost atmospheric and thus the flow is stagnant there. The leading edge of the concave surface of the returning blade is affected by the wake of the advancing blade. Thus, almost stagnation pressure occurs nearly at $\phi_r = -30^\circ$ and it decreases as the flow accelerates over the surface up to $\phi_r = 70^\circ$. Then the flow separates at around $\phi_r = -80^\circ$. On the concave surface of the returning blade the pressure is approximately constant at a negative value. So there are two separation points on the convex surface, one at the advancing blade and the other at the returning blade. With increasing rotor angle these separation points move towards the leading and trailing edges of the advancing blade and returning blade respectively. This is confirmed in Fig. 3(b) for $\alpha = 45^\circ$ and in Fig. 3(c) for $\alpha = 90^\circ$. Beyond $\alpha = 90^\circ$, flow separates at the trailing edge of the advancing blade and on the surface of the returning blade (Fig. 3(d)). The effect of the overlapping gap on the pressure distribution is prominent from any rotor angle except for $\alpha = 0^\circ$.

The drag coefficients, C_n and C_t are shown in Fig. 4 for different rotor angles. The results are compared with those of Sawada et al [4]. The variations of C_n and C_t with α are similar in both cases, but maximum deviations are found at rotor angle from 60° to 120° for C_n and around $\alpha = 240^\circ$ for C_t. This may be the effect of the slightly different S and a large difference in the Reynolds number. Again, C_n and C_t produce a resultant thrust on the support of the rotor and this resultant thrust reaches its maximum value at $\alpha = 120^\circ$ and its minimum value at $\alpha = 0^\circ$. The drag coefficient $C_n(\alpha)$ for the advancing blade which is responsible for the torque production, is positive for a rotor angle of 0° to 150° and reaches its maximum value between 30° to 120°. Between $\alpha = 150^\circ$ and $\alpha = 180^\circ$, $C_n(\alpha)$ becomes slightly negative. The drag coefficient $C_n(\alpha + 180^\circ)$, for the returning blade, is small compared to that of the advancing blade. Drag coefficient C_n for the returning blade is positive, i.e. it is in favour of torque production from $\alpha = 0^\circ$ to $\alpha = 70^\circ$, but

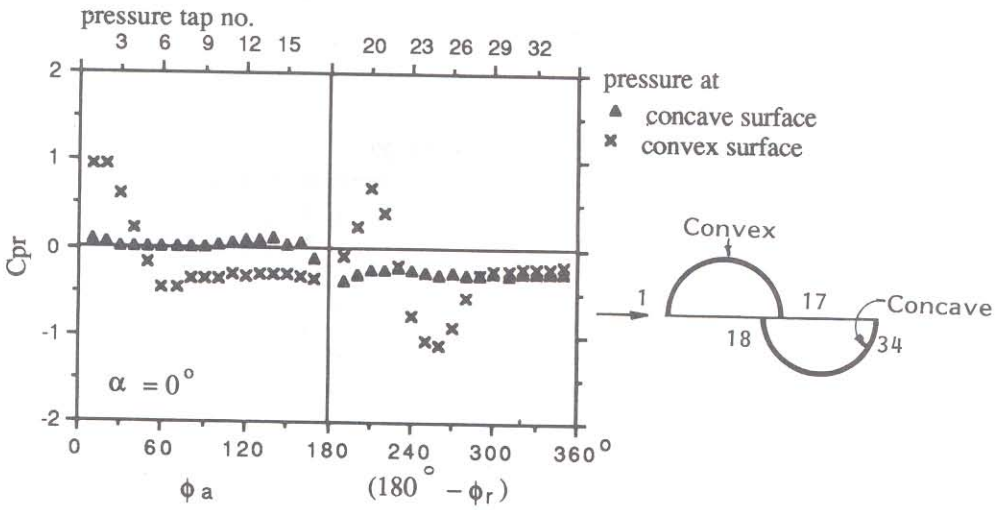

Fig. 3(a). Pressure distribution over the blade surfaces.

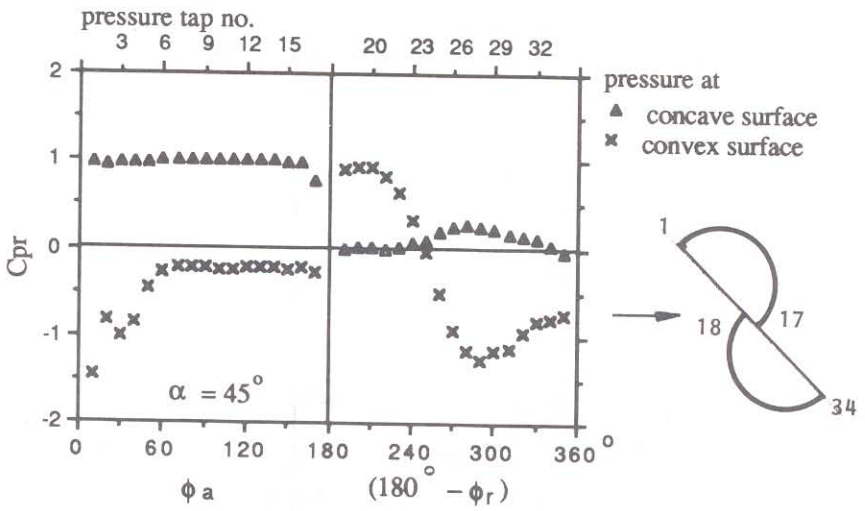

Fig. 3(b). Pressure distribution over the blade surfaces.

beyond $\alpha = 70°$ it produces negative torque. This is illustrated in Fig. 5. Figure 6 shows the total static torque coefficient, C_Q for different rotor angles, and the results are compared with those of Sawada et al. [4] and Fujisawa [5]. The maximum static torque occurs around 45° of rotor angle and this is also supported by other research. A negative torque is produced at $\alpha = 165°$ to $\alpha = 180°$. A negative torque is also found by Fujisawa [5] between $\alpha = 135°$ to $\alpha = 165°$. Sawada et al [4] did not find any negative torque but around this rotor angle it was minimal.

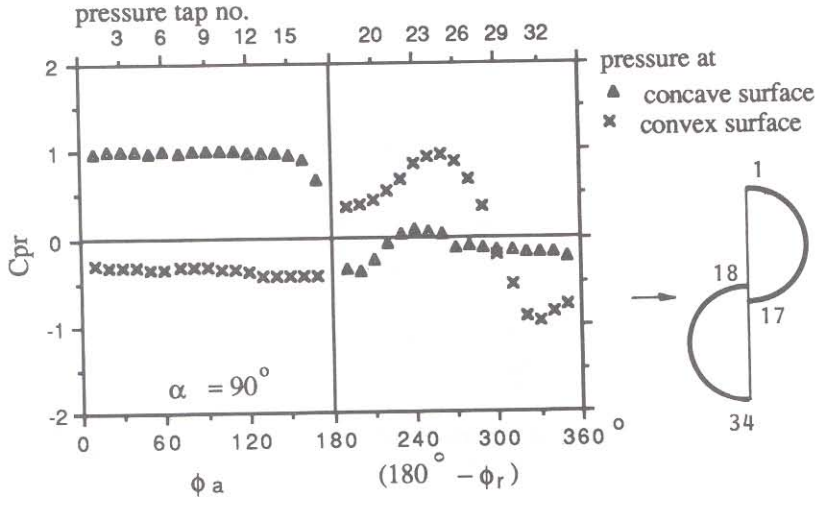

Fig. 3(c). Pressure distribution over the blade surfaces.

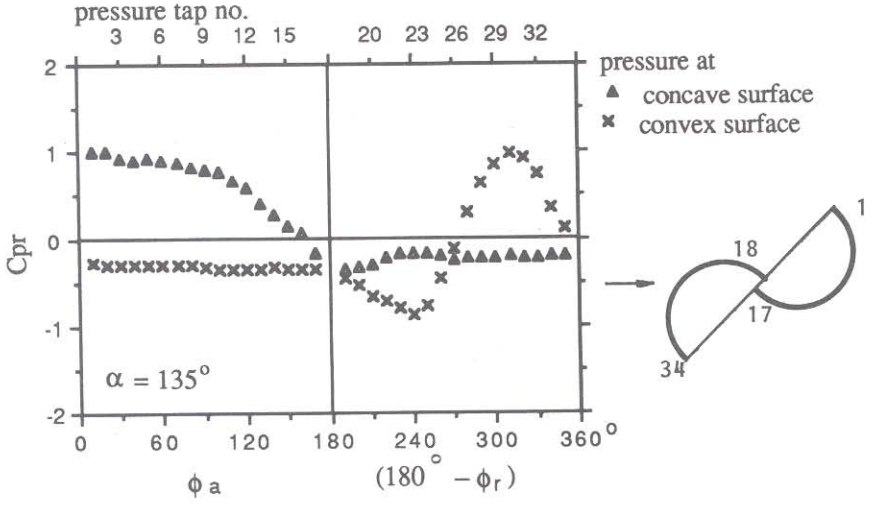

Fig. 3(d). Pressure distribution over the blade surfaces.

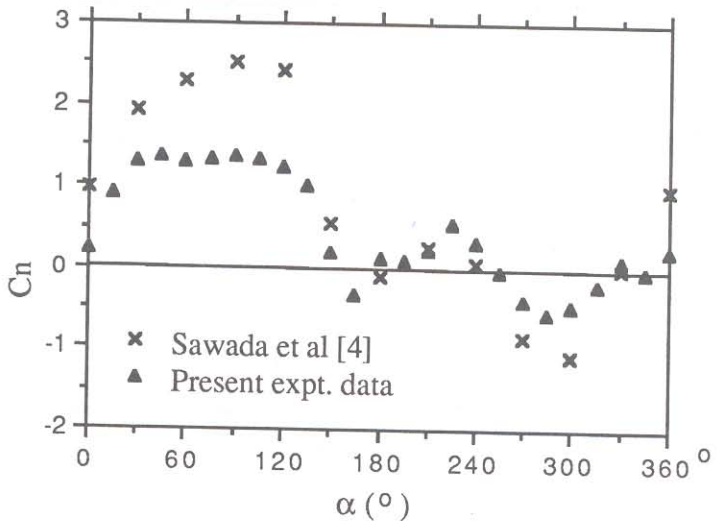

Fig. 4(a). Drag coefficients at different rotor angles.

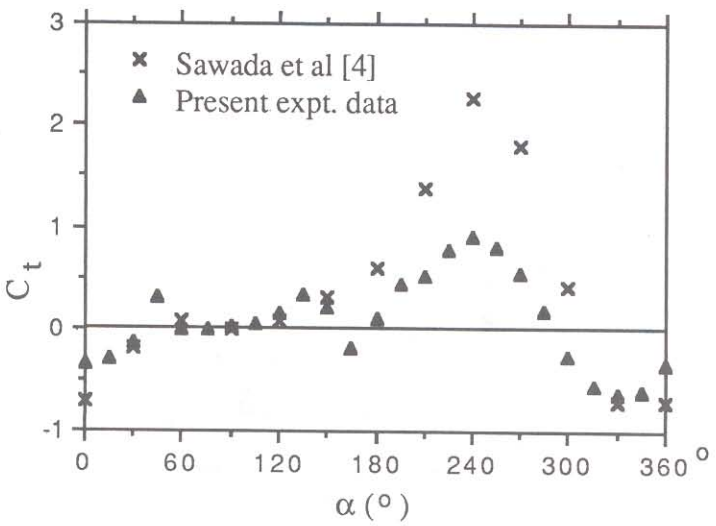

Fig. 4(b). Drag coefficients at different rotor angles.

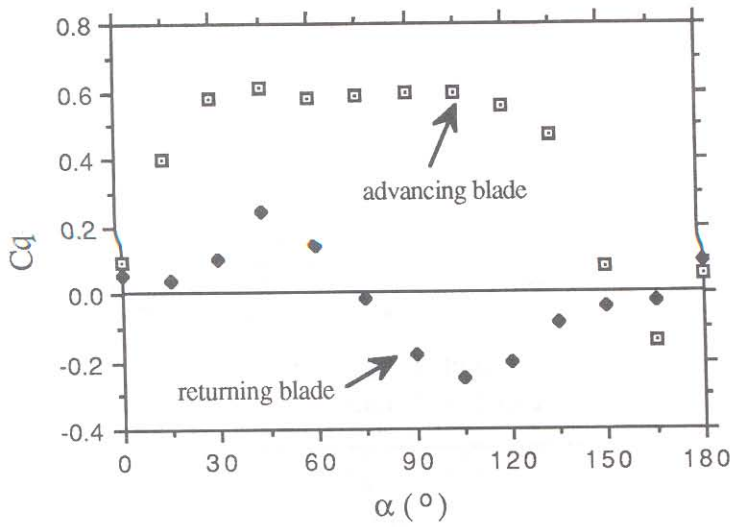

Fig. 5. Torque coefficients for individual blade with different rotor angle.

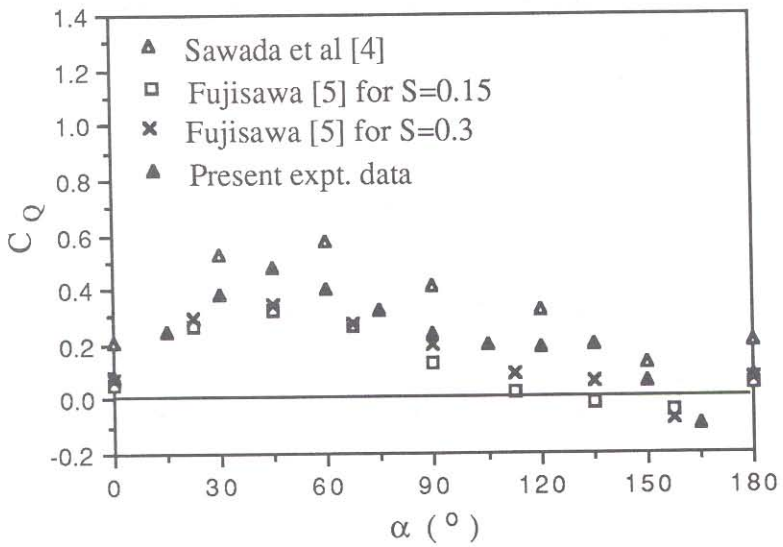

Fig. 6. Total static torque coefficient at different rotor angle.

Prediction of Power Coefficient

The quasi-steady approach applied to the analysis of a Darrieus rotor has been considered for predicting the performance of the Savonius rotor. The static drag coefficient obtained experimentally at a blade angle α, has been used in conjunction with the relative velocity V_r corresponding to a particular tip speed ratio λ to evaluate the force acting on the blade. The power coefficient has been estimated by averaging the work done over a cycle. Figure 7 illustrates the velocity triangles for the advancing and returning blades. The following equations have been used to estimate the power coefficient at a blade angle α.

$$C_n'(\alpha) = C_n(\alpha) * \left(V w_a / U_o\right)^2 \tag{6}$$

$$C_n'(180 + \alpha) = C_n(180 + \alpha) * \left(V w_r / U_o\right)^2 \tag{7}$$

Torque coefficient at α,

$$C_Q'(\alpha) = \left[C_n'(\alpha) + C_n'(180 + \alpha)\right] \frac{1 - S}{(2 - S)^2} \tag{8}$$

Power coefficient at α,

$$C_p(\alpha) = C_Q'(\alpha) \cdot \lambda \tag{9}$$

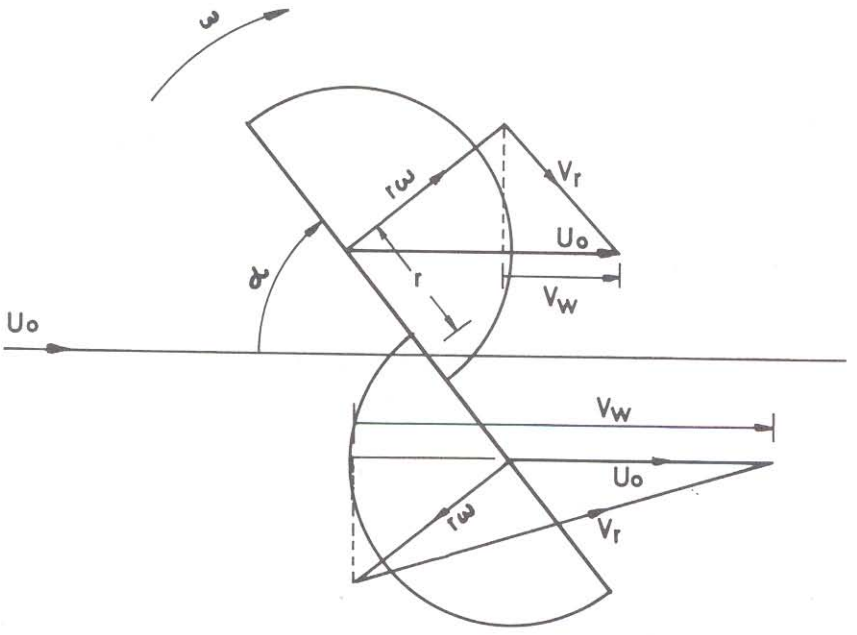

Fig. 7. Typical velocity triangles combining the effect of free stream velocity and blade rotation.

The predicted power coefficients for different tip speed ratios are shown in Fig. 8 along with the measured data of Ogawa & Yoshida [11]. The rotor of Ogawa & Yoshida has the same overlap ratio of the one considered in this study. The predicted power coefficient matches qualitatively with the measured data, but shows a great deviation. The present prediction method assumes a potential vortex, however, in reality the flow field around a rotating rotor is governed by time dependent shear layers, separated flows and high turbulence levels. Furthermore, the wake has not been considered in the present study. However, further research considering the complex flow behaviour may give a better prediction of the performance of a Savonius rotor.

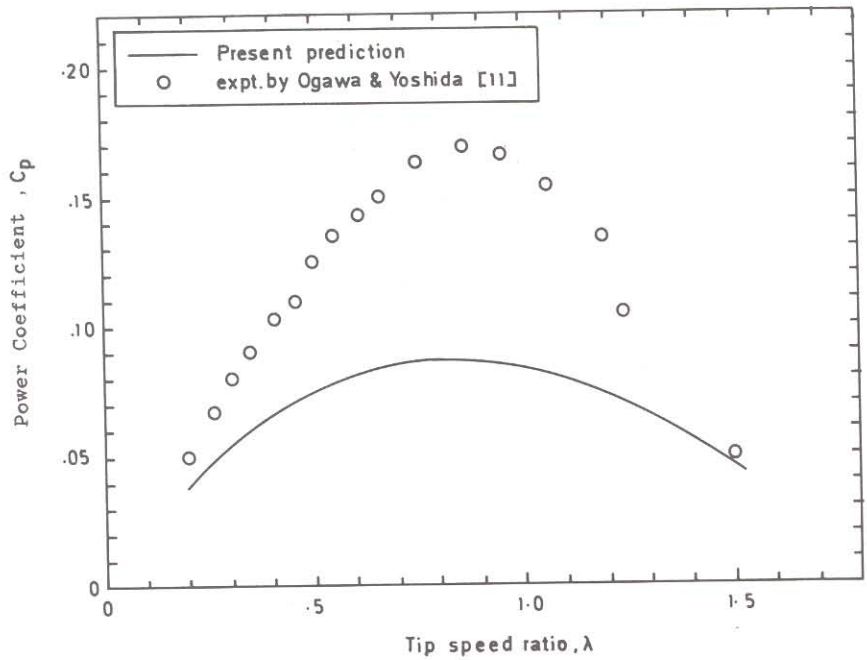

Fig. 8. Results of quasi-steady approach.

CONCLUSIONS

The pressure distribution and the torque mechanism of a Savonius rotor having two semi-circular blades with an overlap ratio $S = 0.2$ have been investigated experimentally. The results can be summarized as follows :

(1) Flow separates over the convex surface of the blades and the separation point moves towards the leading and trailing edges of the advancing and returning blades respectively as the rotor angle increases from 0° to 90°. Beyond $\alpha = 90°$, flow separates on the convex surface of the returning blade only.

(2) The difference in pressure on the convex and concave surfaces, produces drag coefficients, C_n and C_t in the normal and tangential directions of the chord. Drag coefficients C_n and C_t are a function of rotor angle and their resultant reaches maximum value at $\alpha = 120°$ and minimum value at $\alpha = 0°$.

(3) The returning blade acts in favour of the torque production for rotor angles of 0° to 70°, beyond 70° this blade acts against the rotation. Thus, the maximum static torque occurs at around 45°. The static torque becomes negative at $\alpha = 150°$ to 180°.

(4) The quasi-steady approach gives a qualitative prediction of the performance of a Savonius rotor with the measured static pressure coefficients. Further research should be carried out incorporating the complex fluid flow behaviour around the rotor for better prediction of the dynamic behaviour.

REFERENCES

1. Lysen, E.H., H.G. Bos, and E.H. Cordes (1978), *Savonius Rotors for Water Pumping*, SWD Publications, P.O. Box 85, Amersfoort, The Netherlands.
2. Sivasegaram, S. (1977), Design Parameters Affecting the Performance of Resistance Type Rotors, *Wind Engineering*, Vol.1, pp.207-217.
3. Newman, B.G. (1974), Measurements on a Savonius Rotor with a Variable Gap, *Proc. Symposium on Wind Energy: Achievements and Potential*, Sherbrooke, Canada.
4. Sawada, T., M. Nakamura and S. Kamada (1986), Blade Force Measurement and Flow Visualization of Savonius Rotors, *Bulletin of JSME*, Vol. 29, No. 253.
5. Fujisawa, N. (1992), On the Torque Mechanism of Savonius Rotors, *J. of Wind Engg. & Ind. Aero.*, Vol. 40, pp.277-292.
6. Lysen, E.H. (1983), *Introduction to Wind Energy*, Steering Committee of Wind Energy for Developing Countries, P.O. Box 85, Amersfoort, The Netherlands.
7. Islam, M.Q. (1986), *A Theoretical Investigation of the Design of Horizontal Axis Wind Turbines*, Ph.D. Thesis, Vrije Universiteit Brussel, Belgium.
8. Beurskens, H.J.M. (1980), Low Speed Water Pumping Windmills: Rotor Tests and Overall Performance, *Proc. of Third International Symposium on Wind Energy Systems*, 26-29 August, Copenhagen, Denmark.
9. Wilson, R.E. and S.N. Walker (1981), *Performance Analysis Program for Propeller Type Wind Turbines*, Oregon State University, March, USA.
10. Park, J. (1975), *Simplified Wind Power Systems for Experimentry*, Helion Inc., Brownsville, California, USA.
11. Ogawa, T. and H. Yoshida (1986), The Effects of a Deflecting Plate and Rotor End Plates, *Bull. JSME*, Vol. 29, pp.2115-2121.

NOMENCLATURE

a overlap distance

Cp power coefficient

C_{pr} pressure coefficient, $2(p-pa)/\rho U_o^2$

C_n drag coefficient in the normal direction of the chord

C_t drag coefficient in the transverse direction of the chord

C_q static torque coefficient for a single blade

C_Q total static torque coefficient

d diameter of blade

D diameter of the rotor

F_n normal force acting on a blade

F_t tangential force acting on a blade

H height of rotor

p pressure on blade

pa atmospheric pressure

Re Reynolds number, $U_o D/\nu$

S ratio of overlap distance to diameter of blade

T static torque on a blade

U_o free stream velocity

Vr relative velocity

Vw component of relative velocity along U_o

Greek Symbols

α rotor angle

ϕ angle of the pressure tappings

λ tip speed ratio, $\frac{D\omega}{2U_o}$

ω angular speed of the rotor

ν kinematic viscosity

Δp difference of pressure between concave and convex surfaces of a blade

Superscript

dynamic condition